

# Microwave Discharge Ion Sources

*L. Celona*

Istituto Nazionale di Fisica Nucleare, Laboratori Nazionali del Sud, Catania, Italy

## Abstract

This chapter describes the basic principles, design features and characteristics of microwave discharge ion sources. A suitable source for the production of intense beams for high-power accelerators must satisfy the requirements of high brightness, stability and reliability. The 2.45 GHz off-resonance microwave discharge sources are ideal devices to generate the required beams, as they produce multimilliampere beams of protons, deuterons and singly charged ions. A description of different technical designs will be given, analysing their performance, with particular attention being paid to the quality of the beam, especially in terms of its emittance.

## 1 Introduction

The production of high-current beams is a key requirement for various applications, and this is expected to increase in coming years, either for industrial applications or for research projects. High-current and high-brightness  $H^+$  beams can be provided by microwave discharge ion sources (MDISs), which present many advantages in terms of compactness, high reliability, ability to operate in continuous-wave (CW) or pulsed mode, reproducibility and low maintenance. Some applications based on intense proton beams [1] are as follows:

- accelerator-driven systems (ADSs) for nuclear waste transmutation and energy production,
- radioactive ion beams,
- intense neutron spallation sources,
- radiation processing, and
- neutrino factory.

The main parameters of the related proton drivers are listed in Table 1, while Table 2 shows a list of projects (operating and under construction) using high-current proton beams or intense  $H^-$  sources with low transverse emittance.

**Table 1:** Proton driver requirements.

Proton driver	Energy (GeV)	Beam power (MW)
ADS: XADS	$\sim 0.6$	$\sim 5$
Ind. burner	$\sim 1$	$\sim 50$
Spall. neutron source (ESS)	1.33	5
Irradiation facility	1	$> 10$
Neutrino factory (CERN)	2.2	4
RIB: ‘one stage’	$\sim 0.2$	$\sim 0.1$
‘two stage’	$\sim 1$	$\sim 5\text{--}10$

The optimization of beam formation and transport through the low-energy beam transport (LEBT) plays a fundamental role in the provision of a high-quality beam to the accelerator. This is a common requirement of the projects reported in Table 2, where emittances at the entrance to the radio frequency

**Table 2:** High-power accelerator requirements.

	$p/H^-$	mA	ms	Hz	Duty factor (%)	$\pi$ mm mrad
LEDA	p	100	CW	CW	100	0.25
IPHI	p	100	CW	CW	100	0.25
TRASCO	p	30	CW	CW	100	0.2
ESS	p	60/90	2.84	14	4	0.3
SPL	$H^-$	50	1.5	50	7.5	0.2
SNS	$H^-$	50	1	60	6	0.25
JKJ	$H^-$	30	0.5	50	2.5	0.25

quadrupole (RFQ) of the order of 0.20–0.30  $\pi$  mm mrad are needed, making it essential to design and test the ion source and LEBT as a whole. The major challenge of the accelerator front-end is therefore the preparation of a high-quality beam, with a pulse that is well defined in time and has a small transverse emittance. In the following, a review of the major experiences in the production of intense proton beams are reported (Table 2) together with future perspectives.

## 2 Microwave ion source for high-intensity proton production

### 2.1 Historical notes

The history of 2.45 GHz high-current source (HCSs) started about 35 years ago with different source designs proposed by Sakudo [2] and by Ishikawa *et al.* [3], especially for industrial applications. The sources produced remarkable results not only for protons, but also for deuterons and singly charged light ions. A simple concept of the microwave discharge source was based on a non-confining magnetic field higher than the resonance field (i.e. 87.5 mT). Sakudo and his collaborators at the Central Research Laboratory of Hitachi Limited pioneered the development of high-current microwave ion sources for ion implantation [4]. The first Hitachi ion source (see Fig. 1) is composed of a plasma generator, that is, essentially, a section of coaxial waveguide with an axial magnetic field supplied by three solenoids. The 2.45 GHz microwaves are introduced via a water-cooled antenna connected to the inner conductor of a coaxial-to-rectangular waveguide transition. The magnetic induction is varied along the length of the antenna to match the impedance of the plasma-filled chamber to the impedance of the microwave line [5]. The extraction system is a multiaperture triode with 124 apertures 3 mm in diameter distributed over a 50 mm diameter circle. The sources built by Sakudo's group were able to supply 2 mA of  $As^+$  and 15 mA of  $B^+$ , and they were successfully adapted to industrial application setups.

The second microwave ion source developed by Sakudo *et al.* was especially designed to generate a slit-shaped ion beam. The plasma chamber illustrated in Fig. 2 is a tapered ridged waveguide with all but the volume between the ridges filled with boron nitride. The 2.45 GHz microwaves are introduced through a dielectric window from a rectangular waveguide. The electric field between the ridges is relatively uniform, ensuring a reasonably constant plasma density over the entire length.

A step forward was made by Ishikawa [6], whose design was very compact (chamber diameter was 50 mm) and the source was able to produce milliamper beams of any species, finding applications not only in ion implantation devices but also for ion beam deposition. The absence of antennas made this equipment more reliable for long-time operations.

### 2.2 The CRNL ion source

In 1991 a simple and robust design was proposed by Taylor and Mouris at Chalk River National Laboratory (CRNL; see Fig. 3). This source can be considered as the basis of all the different designs proposed

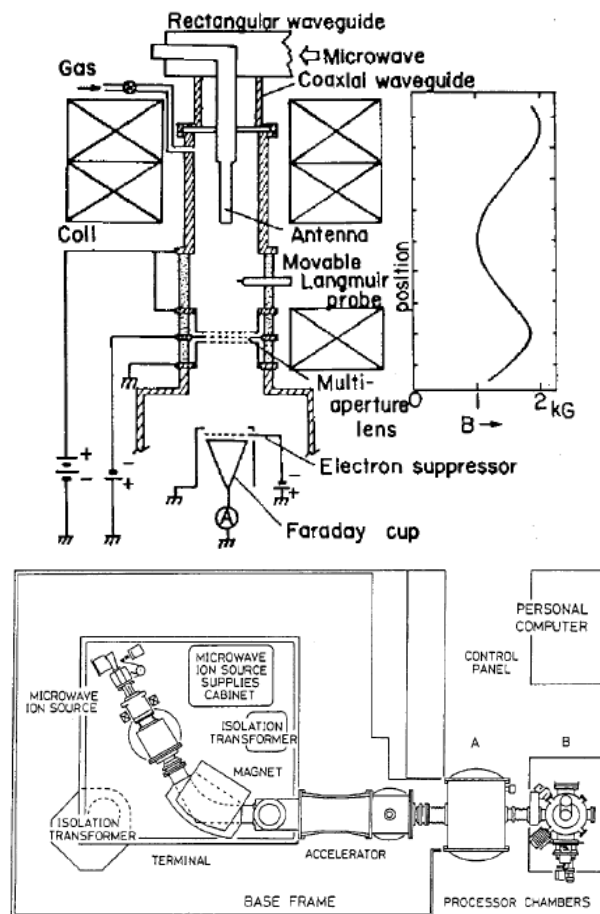


**Fig. 1:** Hitachi microwave ion source with multiaperture extraction system

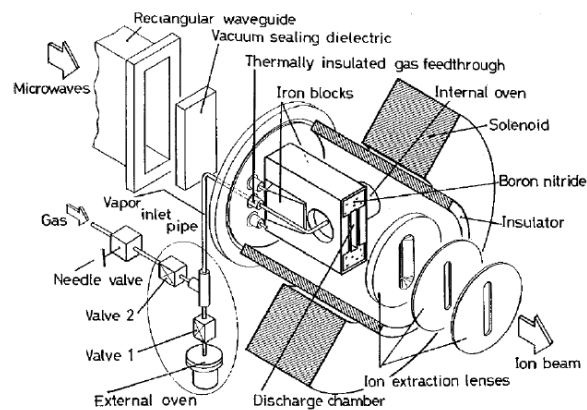


**Fig. 2:** Hitachi microwave ion source with slit extraction system

in the past 25 years. The main innovation consisted in the use of a matching unit to adapt the waveguide to plasma impedance, which enhanced the plasma density and finally the current density of the extracted beam. Moreover, two separately fed solenoids, approximately placed at the two extremes of the plasma chamber, allowed the magnetic field profile to be adapted. The extraction system was not sophisticated but adequate for high-current beam formation, using the three electrodes in the accelerate–decelerate operation mode.

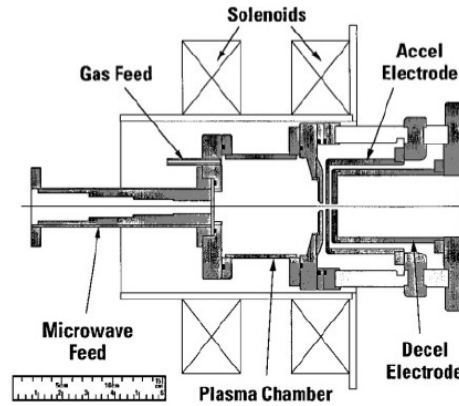


**Fig. 3:** The CRNL microwave source

The configuration of the Chalk River electron cyclotron resonance (ECR) proton source is illustrated in Fig. 4. The plasma generator is simply a hydrogen-filled chamber, with a ceramic rectangular waveguide window, encircled by two solenoids. The extraction system is a 50 kV multiaperture triode.

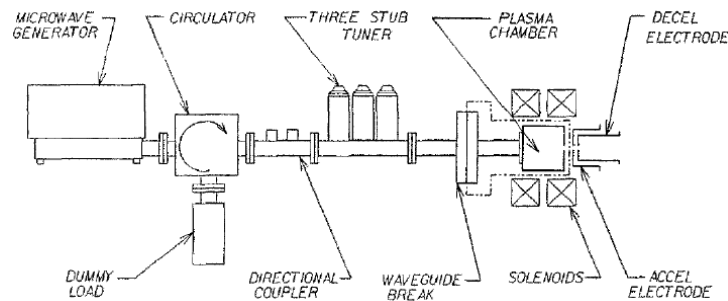


**Fig. 4:** The CRNL microwave source

The microwave line is isolated from the plasma chamber by a d.c. waveguide break consisting of a Teflon sheet sandwiched between a choke flange and a standard flange. Since the solenoids are also electrically isolated from the plasma chamber, only the plasma chamber itself remains at high voltage. All of the power supplies, d.c. as well as microwave, are at ground potential. The ion source generates beam current densities of up to  $350 \text{ mA cm}^{-2}$  at a microwave power of 1000 W. The three-stub tuner is adjusted to optimize the impedance match. Figure 5 illustrates the evolution of the beam current with the mass flow, microwave power and magnetic induction on the plasma chamber axis.

### 2.3 The LEDA injector

This design was further improved by J. Sherman and co-workers at Los Alamos National Laboratory (LANL), who improved the extraction system and the LEBT in order to optimize the beam coupling to the

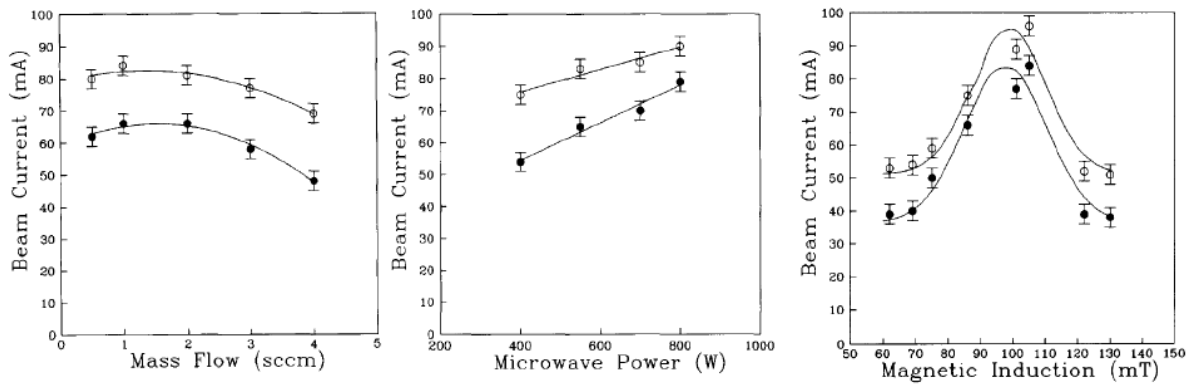


**Fig. 5:** Beam current as a function of mass flow, microwave power and magnetic induction

RFQ of the LEDA project. Then the CRNL plasma generator was integrated with a 75 kV acceleration structure at Los Alamos (Fig. 6) [7]. Plasma is generated by the interaction of 2.45 GHz microwaves with  $H_2$  gas in the presence of an approximate 875 G axial magnetic field.

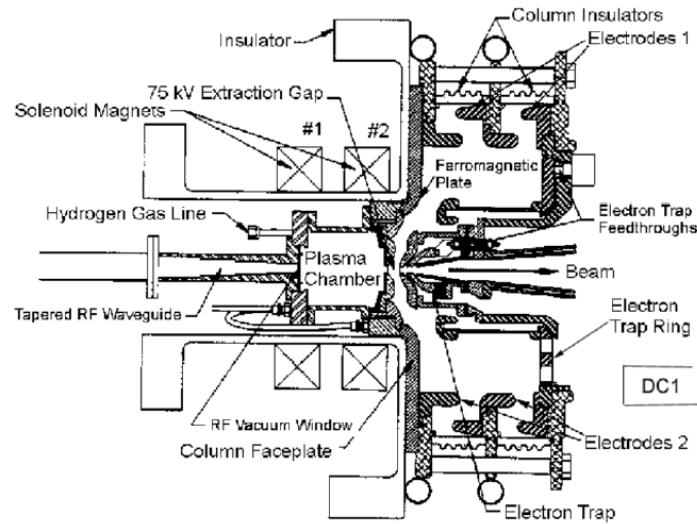


**Fig. 6:** Line drawing of the 75 keV microwave proton source

Beam measurements were made on a prototype injector shown in Fig. 7. The proton source is mounted on a beam diagnostics and pump box, which is followed by two solenoids. The beam current is characterized by two d.c. current monitors (DC1 and DC2), an a.c. beam current transformer for beam noise measurements, an  $x$  and  $y$  video profile system for beam position and width measurements, and an emittance measuring unit (EMU), which also serves as the beam dump. The typical operating parameters of the injector are listed in Table 3.

From Fig. 8 we can see that beam current is measured at DC1, DC2 and in the RFQ entrance collimator for 6.7 MeV RFQ; beam focusing accomplished with LEBT is achieved thanks to solenoid magnets S1 and S2; and beam centroid is controlled with steering magnets SM1 and SM2.

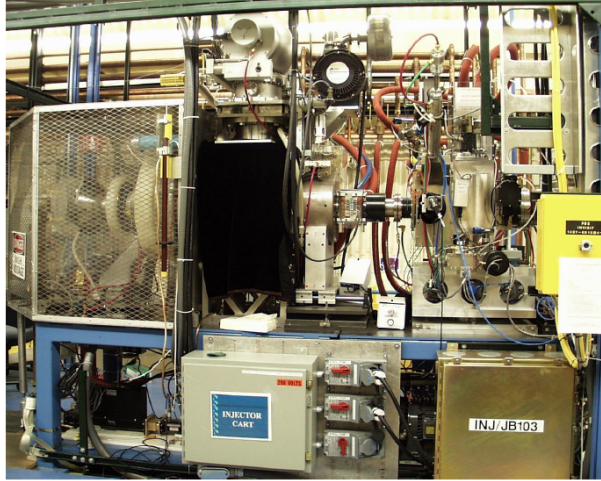


**Fig. 7:** Injector used for the beam measurements

**Table 3:** LEDA injector parameters.

Injector parameter	Value
H <sub>2</sub> gas flow	4.1 sccm*
Ion source pressure	2 mTorr
Ion source gas efficiency	24%
Discharge power, at 2.45 GHz	1.2 kW
Beam energy	75 keV
High-voltage power supply current	165 mA
DC1 current	154 mA
DC2 current	120 mA
Proton fraction	90%
Injector emittance, 1 r.m.s. norm.	0.18 $\pi$ mm mrad

\*sccm = standard cubic centimetres per minute.

## 2.4 The SILHI source

Following the same track, at CEA-Saclay (Commissariat à l'Énergie Atomique, Saclay), the SILHI source obtained large brightness and high reliability in the second half of the 1990s. All the parts of the source, which is shown in Figs. 9 and 10, are robustly engineered, including the beam line elements and diagnostics, adapted to beams exceeding 10 kW, typically 95 kV, 140 mA. A proton/deuteron fraction above 80% and an emittance below 0.2  $\pi$  mm mrad have been obtained, while the reliability has increased over the years, even reaching 99.9% in a one-week test. The SILHI source (see Fig. 10) has been developed at CEA-Saclay, in the framework of the IPHI project, devoted to the production and acceleration of intense proton beams (currents up to 100 mA). The source design and results are described in detail elsewhere [8–10], and in Table 4 we report the main features.

A collaboration arranged between CEA and the Istituto Nazionale di Fisica Nucleare (INFN) has allowed in recent years a significant increase of beam quality produced by SILHI, reaching the outstanding value of 0.1  $\pi$  mm mrad for 0.75 mA as described in detail in the next section.

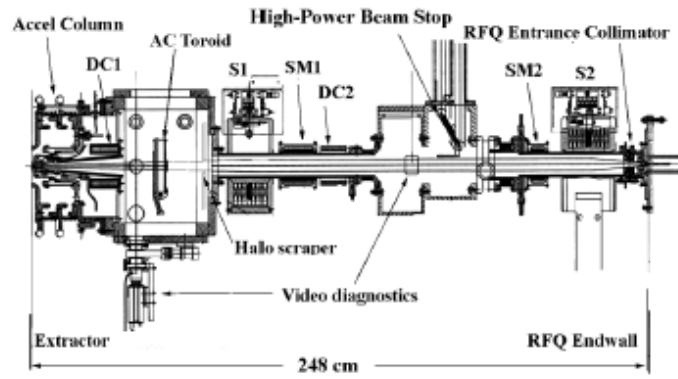


**Fig. 8:** Injector used for the beam measurements

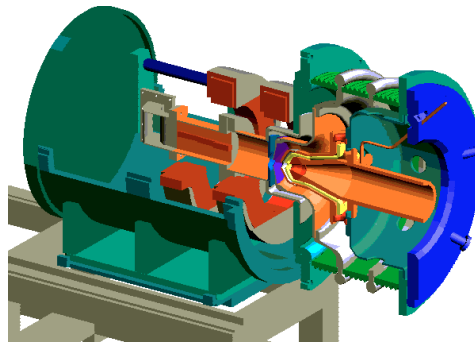


**Fig. 9:** Render view of the SILHI source operating at CEA

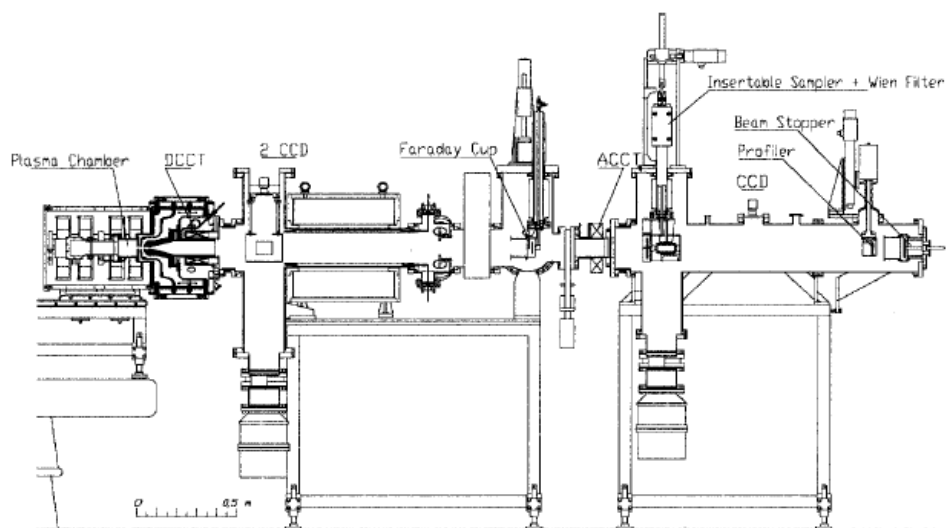


**Fig. 10:** Layout of the SILHI ion source and the beam line

**Table 4:** SILHI source typical operating parameters.

Parameter	Value
Total beam current	140 mA
Proton fraction	$\sim 85\%$
Beam density	$220 \text{ mA cm}^{-2}$
Beam energy	95 keV
Discharge RF power, at 2.45 GHz	1.2 kW
Beam emittance, at 75 mA	$0.1 \pi \text{ mm mrad}$
Hydrogen mass flow	$\sim 2 \text{ sccm}$

## 2.5 TRASCO Intense Proton Source (TRIPS) at INFN-LNS

The TRIPS ion source [11] has been designed, realized and commissioned at INFN-LNS, within the framework of the TRASCO Project (an R&D programme, the goal of which was the design of an accelerator driving system (ADS) for nuclear waste transmutation). With reference to the three experiments outlined above, a series of innovations were implemented on the TRASCO project. The goal of TRIPS was less demanding in terms of currents than it was for the other projects in Table 2, but there was a very strong requirement for source reliability, with an r.m.s. normalized emittance below  $0.2 \pi \text{ mm mrad}$  for an operating voltage of 80 kV (Table 5).

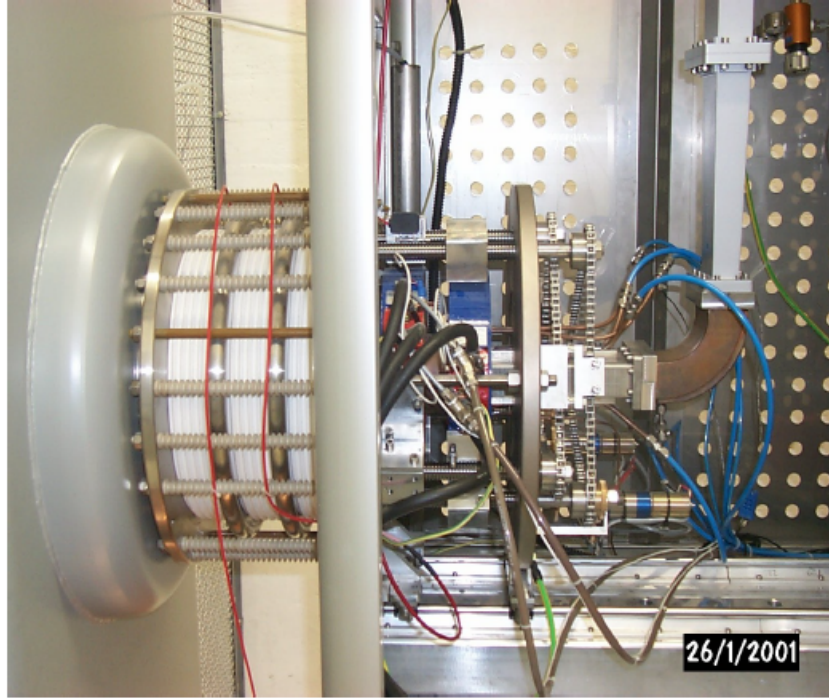
**Table 5:** TRIPS typical operating parameters.

Parameter	Value
Total beam current	60 mA
Proton fraction	90%
Beam energy	80 keV
Microwave power, at 2.45 GHz	0.3–1 kW
Beam emittance, at 35 mA	$0.07 \pi \text{ mm mrad}$
Gas flow	0.4–0.6 sccm
Duty factor, at 35 mA	99.8%
Reliability, at 35 mA	99.8%

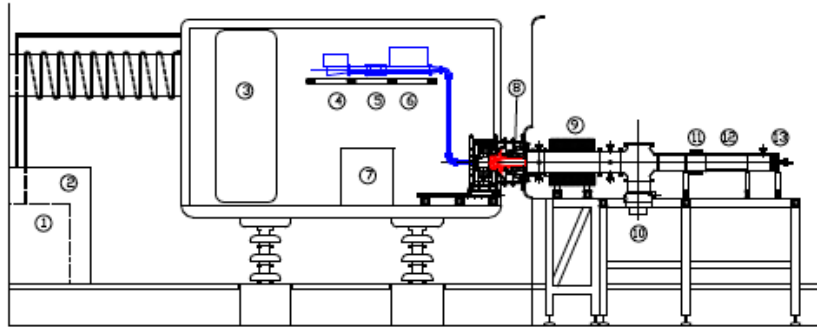
The major innovation consisted in the use of two movable coils permitting the magnetic field profile to be varied. The plasma chamber dimension and the four-step matching transformer were defined to get a uniformly dense plasma at the extraction hole (6 or 8 mm diameter). The microwave coupling with the matching transformer and the automatic tuning unit allowed operation with low values of reflected power (below 5%) and a high electric field on the axis, thus increasing proton fraction and current density, up to  $200 \text{ mA cm}^{-2}$ . The extraction system was designed in collaboration with Saclay, exploiting the experience already gained at INFN-LNS for the design of extraction geometries from plasma sources. Measurements with the 8 mm hole plasma electrode have given results largely exceeding the TRASCO design current: up to 61 mA were extracted at 80 kV and about 90% of the beam has been transported to the beam stop.

Figure 11 shows the TRIPS source and Fig. 12 shows the experimental set-up. The first section of the low-energy beam transfer line (LEBT) devoted to beam analysis consists of a current transformer (DCCT1), a focusing solenoid, a four-sector ring to measure beam misalignments and inhomogeneities, a second current transformer (DCCT2) and an insulated 10 kW beam stop (BS), which measures the beam current.





**Fig. 11:** The TRIPS ion source on the 100 kV platform



**Fig. 12:** The experimental set-up: (1) demineralizer; (2) 120 kV insulating transformer; (3) 19 inch rack for the power supplies and for the remote control system; (4) magnetron and circulator; (5) directional coupler; (6) automatic tuning unit; (7) gas box; (8) DCCT1; (9) solenoid; (10) turbomolecular pump; (11) DCCT2; (12) quartz tube; (13) 10 kW beam stop.

Systematic measurements with movable coils have been carried out for different positions and currents, by leaving the other parameters unchanged. From these measurements it can be determined that the source is more sensitive to variations in the extraction coil than in the injection one. The best performance is clearly obtained when the two ECR zones are located exactly on the boron nitride discs at the two ends of the plasma chamber. Figure 13 shows the best obtained profile (the straight line represents the value of the magnetic field corresponding to the resonance at 2.45 GHz).

Systematic emittance measurements have been made with an emittance measurement unit provided by the CEA-Saclay SILHI group, showing the effect of each parameter on the beam emittance; more details are reported in the next section.

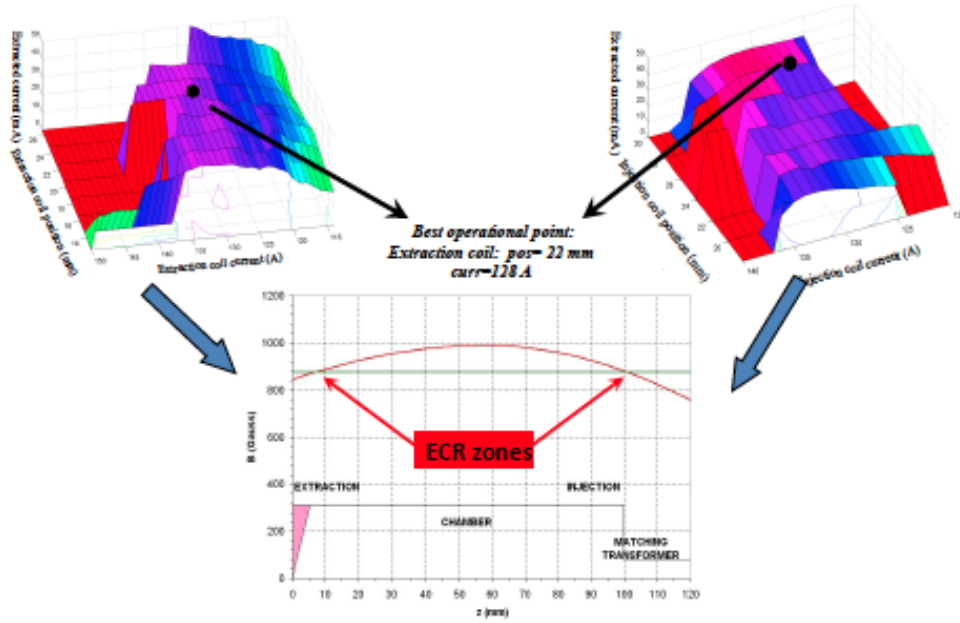


**Fig. 13:** Magnetic field optimization through changes in the coil current and position (above) and ideal profile (below).

## 2.6 Versatile Ion Source (VIS)

The TRIPS source exceeded all the requirements of the TRASCO project, but in order to simplify it, the VIS source was built in 2006 [12]. In particular, in the VIS source, the movable coils have been replaced with permanent magnets, and the extraction geometry and extraction column have been simplified. With these modifications it has been possible to avoid the high-voltage platform and the insulating transformer, by insulating the gas pipe and the waveguide line. All these changes decreased the high-voltage sparks and increased the source reliability. All the devices for the remote control were placed at ground potential, thus leaving only the plasma chamber and the permanent magnets at high voltage. The compact dimensions have also resulted in better and easier maintenance. The magnetic system consists of a set of three Vacodym 745 HR permanent magnets; they are packed together with two soft iron spacers and they are supported by a stainless-steel tube. The layout of the VIS source is reported in Fig. 14 [13].

The microwave line, in Fig. 15, is the result of an optimization study carried out with tools for high-frequency structure simulation in order to reduce microwave losses, simultaneously with an adequate matching of the waves to the plasma chamber. A plasma is generated by means of the microwaves provided by a 2.45 GHz magnetron through a WR 340 (86.4 mm × 43.2 mm) waveguide excited in the TE<sub>10</sub> dominant mode. An automatic tuning unit adjusts the modulus and phase of the incoming wave in order to match the plasma chamber impedance with and without the plasma, and a dual-arm directional coupler is used to measure the forward and the reflected power.

In TRIPS both the microwave line and the microwave generator are placed on the high-voltage platform, while in VIS the microwave generator is placed at ground potential. Then, in order to separate the high-voltage region from the grounded one, a waveguide d.c. break has been designed and realized with the support of the HFSS electromagnetic simulator. It is made of 31 aluminium discs of a WR 340 waveguide insulated from one another by means of fibreglass. The conductive parts will be fixed to voltages gradually decreasing from 80 kV to ground voltage, still keeping the insertion loss low. The high-pressure quartz window is placed before the WR 284 water-cooled copper bend in order to avoid any damage due to back-streaming plasma electrons. Finally, a maximally flat matching transformer has been inserted before the plasma chamber, shown in Fig. 16, which is an optimized version of a similar device

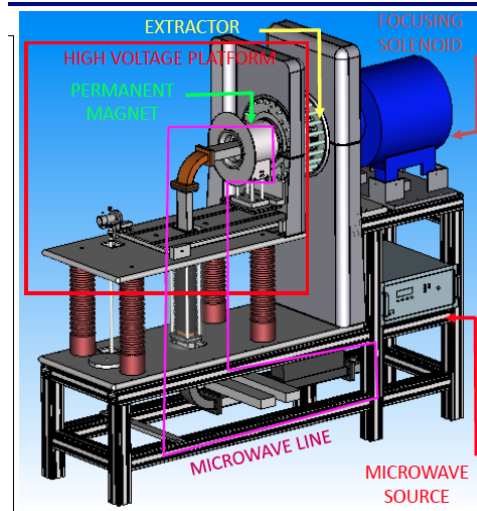


**Fig. 14:** A render view of the VIS source together with the focusing solenoid

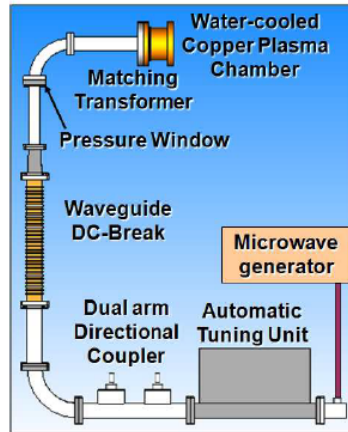


**Fig. 15:** VIS microwave line

used in MIDAS and TRIPS ion source. This realizes an impedance matching with the plasma chamber and concentrates the electromagnetic field near the axis. The enhancement of the electromagnetic field in the plasma chamber cavity increases the plasma density locally and finally the ionization process.

The ionic component of the plasma produced in the plasma chamber is then extracted by means of a four-electrode extraction system. The low-energy beam transport line (LEBT) allows beam analysis, and it consists of a focusing solenoid, a four-sector diaphragm to measure the beam misalignments, a d.c. current transformer, a  $30^\circ$  bending magnet (Fig. 17) and an insulated beam stop to measure the beam current, shown in Fig. 18. The extraction system consists of a plasma electrode made of molybdenum at 65 kV voltage, two water-cooled grounded electrodes and a 3.5 kV negatively biased screening electrode inserted between them, in order to avoid secondary electrons due to residual gas ionization, back-streaming to the extraction area. The VIS extraction has been optimized to work around 40 mA, fulfilling the requirement of high brightness. The beam emittance measurements are described in the next section. The beam availability has been further increased and damage to the electronics because of high-voltage sparks is negligible.

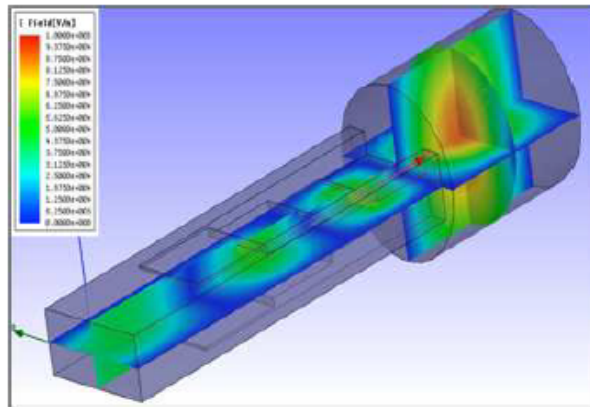


**Fig. 16:** Electric field amplitude at 2.45 GHz

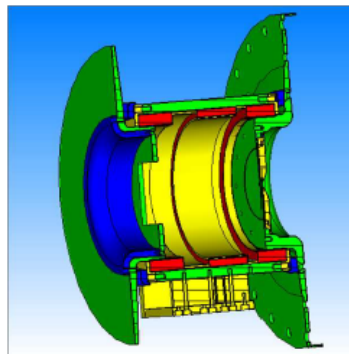


**Fig. 17:** Magnet



**Fig. 18:** VIS beam line

### 3 Beam emittance measurements

The production of a high-quality beam has been, since the first measurements made at CRNL by Taylor and Wills, one of the major challenges for such sources, together with beam reliability. Over the years, many developments have been carried out to improve these aspects, and the most important results have been obtained through a deep optimization of the extraction geometry together with an appropriate design of the low-energy beam transfer line.

#### 3.1 SILHI beam emittance improvements

A significant step forward in this field, namely the production of a high-quality beam, was made within the framework of the collaboration between INFN and CEA, in which an innovative method based on the controlled injection of a gas into the line was developed [14]. The idea is based on the fact that the ions obtained from residual gas ionization are expelled from the centre of the beam line, where the potential is positive, towards the wall. Electrons from the wall are attracted towards the beam, so that the beam is compensated, provided that the pressure is high enough to have an adequate number of electrons (a compromise between beam losses and space-charge compensation is to be found experimentally). According to that approach, the most effective gases are the heaviest, which easily release a large number of electrons. If  $N$  hydrogen atoms per unit volume are required for optimum compensation (i.e. if  $N$  electrons neutralize the beam space charge), for a species that gives  $Z_{\text{eff}}$  electrons when the atoms interact with the 95 keV proton beam, the optimum number of atoms per unit volume is  $N/Z_{\text{eff}}$  (this clue neglects the dissociation process, which does not require a large amount of energy).

Experiments have been carried out by injecting different gases ( $\text{H}_2$ ,  $\text{N}_2$ ,  $^{84}\text{Kr}$  and  $\text{Ar}$ ) into the SILHI beam line through a leak valve placed after the LEBT solenoid and comparing the emittance measurements at different pressures with an extracted beam in range of 75–80  $\mu\text{A}$ . Two gauges (measuring  $p_1$  and  $p_2$ ) are placed, respectively, at the extraction column exit and between the sampler and the profiler in the diagnostic box (Fig. 10). In all the cases considered here, a decrease of beam emittance has been observed with the beam line pressure increase. These results have been explained by a higher degree of space-charge compensation as confirmed by a series of measurements carried out in collaboration with the Los Alamos National Laboratory (LANL).

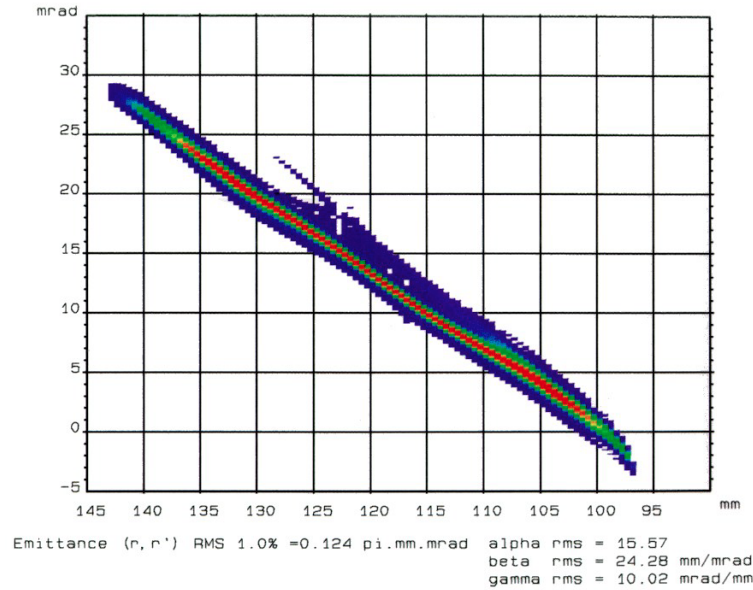


**Fig. 19:** Emittance plot after injecting Ar into the beam line:  $p_1 = 4.5 \times 10^{-5}$  Torr,  $p_2 = 4.4 \times 10^{-5}$  Torr,  $\epsilon_{\text{rms}} = 0.124 \pi \text{ mm mrad}$ .



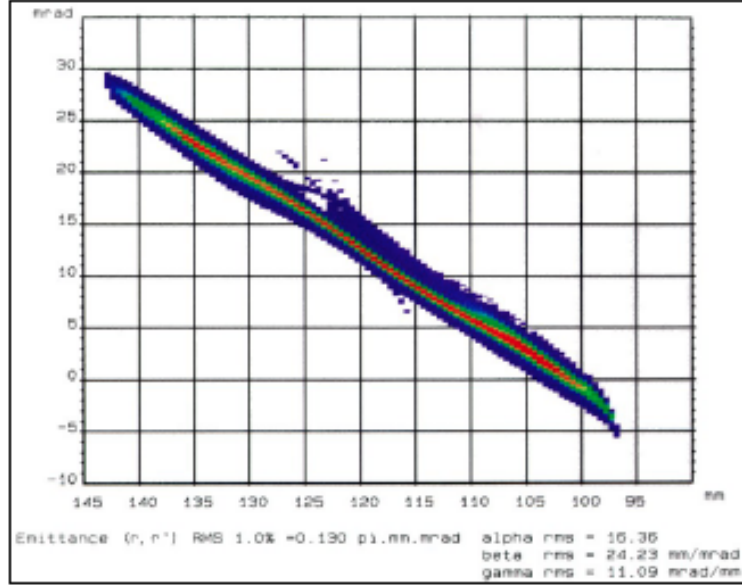


**Fig. 20:** Emittance plot after injecting  $N_2$  into the beam line:  $p_1 = 4.5 \times 10^{-5}$  Torr,  $p_2 = 4.5 \times 10^{-5}$  Torr,  $\epsilon_{\text{rms}} = 0.13 \pi$  mm mrad.

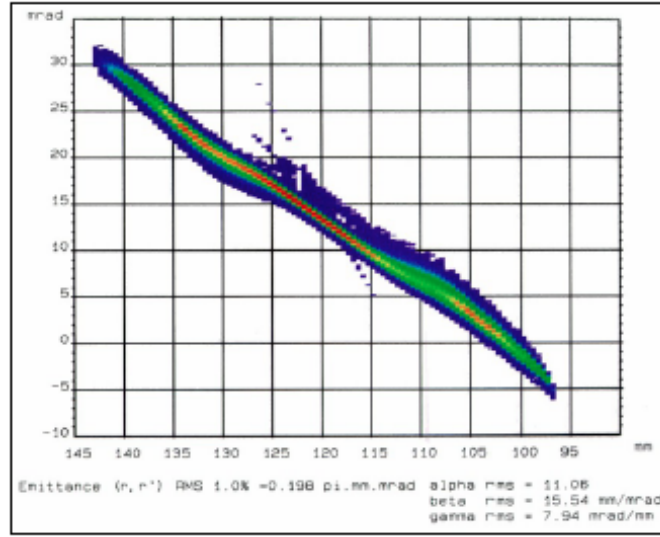


**Fig. 21:** Emittance plot after injecting  $H_2$  into the beam line:  $p_1 = 5 \times 10^{-5}$  Torr,  $p_2 = 4.9 \times 10^{-5}$  Torr,  $\epsilon_{\text{rms}} = 0.198 \pi$  mm mrad.

As observed, the behaviour depends upon the atomic mass of the species injected. In particular, an r.m.s. normalized emittance of  $0.1 \pi$  mm mrad has been obtained with  $^{84}\text{Kr}$  injected into the beam line ( $p_1 = 3 \times 10^{-5}$  Torr). The emittance is reduced by a factor of 3 with respect to the value  $0.33 \pi$  mm mrad measured without gas ( $p_1 = 1.8 \times 10^{-5}$  Torr). Emittance values below  $0.15 \pi$  mm mrad have been easily obtained also using Ar with pressure values of the first gauge around  $2.5 \times 10^{-5}$  Torr. For this gas, the minimum value of r.m.s. normalized emittance of  $0.125 \pi$  mm mrad has been measured (see Fig. 19). A lower efficacy is obtained with  $N_2$  and  $H_2$  injection: in particular, with  $N_2$  injection we have measured  $0.13 \pi$  mm mrad at relatively high pressure ( $p_1 = 4.5 \times 10^{-5}$  Torr; see Fig. 20), while for  $H_2$  the minimum value of emittance obtained is  $0.198 \pi$  mm mrad, as shown in Fig. 21.

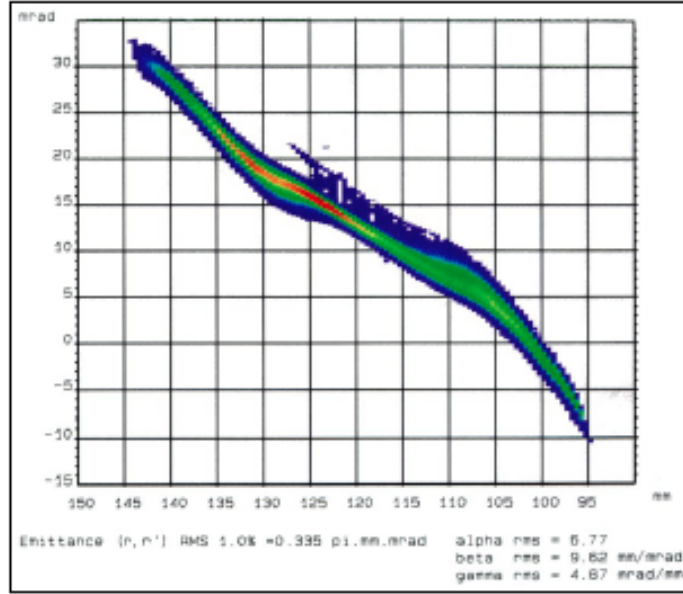


**Fig. 22:** Emittance picture without injecting  $^{84}\text{Kr}$  into the beam line:  $\epsilon_{\text{rms}} = 0.33 \pi \text{ mm mrad}$ ,  $p_1 = 8 \times 10^{-5} \text{ Torr}$ ,  $p_2 = 1.2 \times 10^{-5} \text{ Torr}$ .

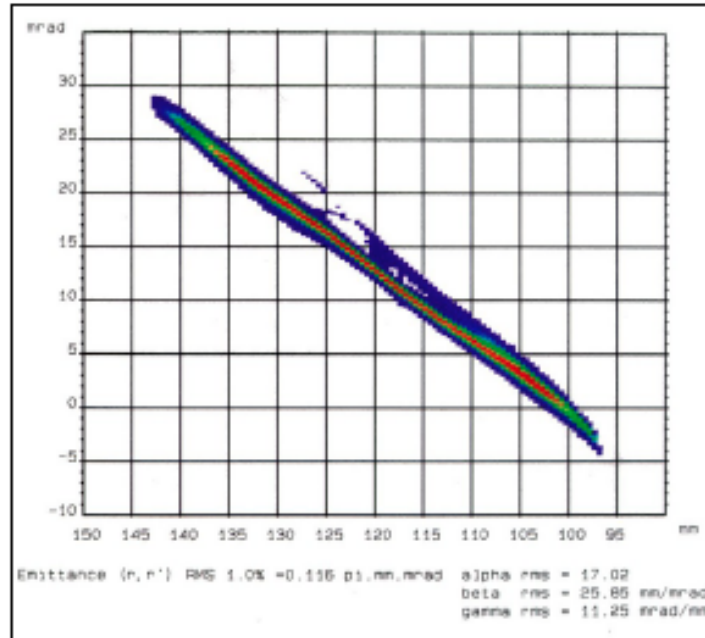


**Fig. 23:** Emittance picture after injecting  $^{84}\text{Kr}$  into the beam line:  $\epsilon_{\text{rms}} = 0.11 \pi \text{ mm mrad}$ ,  $p_1 = 3.5 \times 10^{-5} \text{ Torr}$ ,  $p_2 = 2.7 \times 10^{-5} \text{ Torr}$ .

Figures 22 and 23 show the emittance measurement obtained with  $^{84}\text{Kr}$ . It must be pointed out that the emittance pictures become straight with the gas injection and present a lower beam size and lower aberrations. This is also evident during the measurement because each beamlet selected by the sampler has a lower width and a higher intensity.

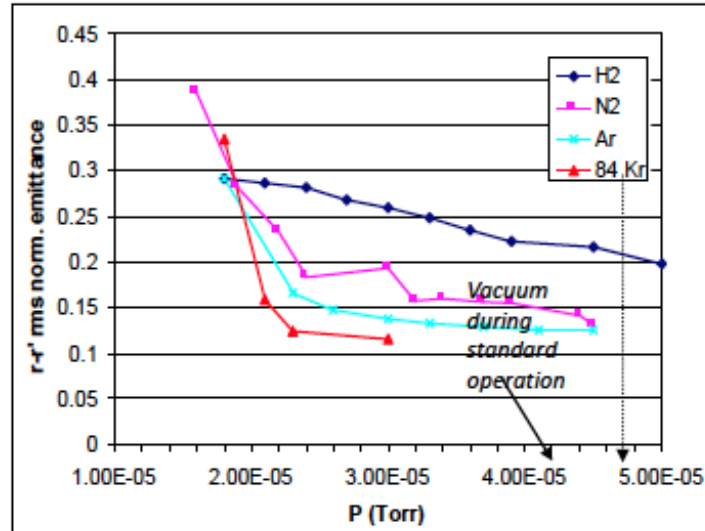


**Fig. 24:** Space-charge compensation with  $\text{H}_2$ ,  $\text{N}_2$ , Ar and Kr

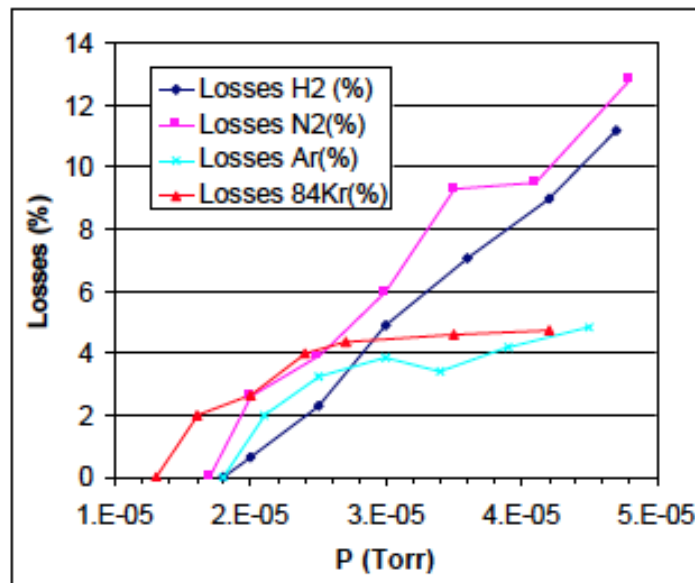


**Fig. 25:** Losses of the beam current

Figure 24 summarizes the results obtained and in all cases a decrease of beam emittance has been observed with the increase of beam line pressure. Figure 25 summarizes also the losses at the end of the beam line at the different pressures, losses that are less than 5% for masses heavier than Ar.



### 3.2 TRIPS beam emittance improvements

The requirement in terms of proton current for the TRIPS source (Table 2) was significantly lower than that for the SILHI source, and therefore (at the nominal beam current) gas injection has been not necessary to achieve the required goal. However, also in this case this method has been important to decrease the emittance at higher currents.

In this case the measured values were coherent with the calculated ones and close to those predicted by the equation

$$\epsilon_{\text{normal,rms}} = \frac{1}{4} \times 0.0653r \left( \frac{kT}{A} \right)^{1/2} \quad (\pi \text{ mm mrad}), \quad (1)$$

where  $r$  is the radius of the extraction aperture in millimetres,  $A$  is the rest mass of the ion in atomic units and  $kT$  is the ion temperature in electronvolts. Assuming an ion temperature of 1 eV and with an extraction hole of 3 mm radius, the expected r.m.s. normalized emittance is circa  $0.05 \pi \text{ mm mrad}$ . The emittance values measured are close to the theoretical one for a beam current close to the nominal value, while at higher currents the space-charge effects play an important role in the beam blowup, and a gas must be added into the beam line to decrease the beam emittance.

Measurements [15] have been carried out at different current levels (between 30 and 50 mA); for a fixed current value, we have explored the effect of some parameters such as puller voltage and solenoid current on the beam emittance. A first observation was that the emittance slightly changes with the puller voltage for a fixed current. Measurements performed on a 42 mA beam, with the solenoid fixed at 290 A, a hydrogen flux of 0.49 sccm and a discharge power of 650 W, show a decrease of emittance from 0.208 to  $0.172 \pi \text{ mm mrad}$  just by increasing the voltage drop between the extraction and puller electrode from 38 to 43 kV. The optimal operating value ranges between 40 and 42 kV; unfortunately, for higher voltage HV discharges occur and it was not possible to operate the source safely. Another important observation was obtained by looking at the evolution of the beam emittance by changing the solenoid strength for fixed source conditions.

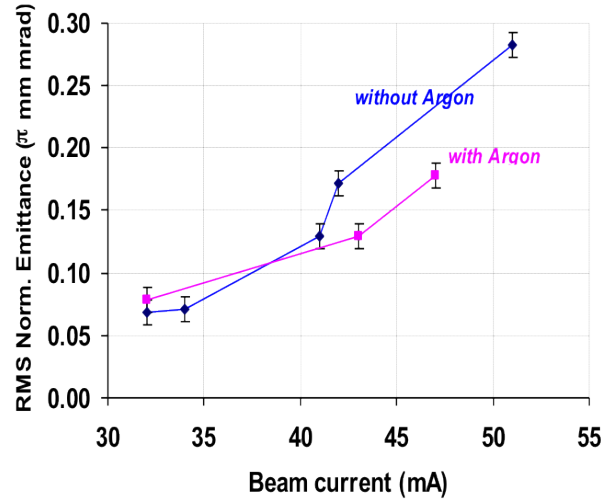


**Fig. 26:** The r.m.s. normalized emittance versus beam current

Measurements were carried out on a 32 mA beam with the puller fixed at 40 kV, the discharge power at 550 W and the hydrogen flux at 0.45 sccm; the emittance changes between 0.069 and  $0.137 \pi \text{ mm mrad}$  by decreasing the solenoid current. This in turn means that the position of the crossover along the beam line is extremely important for the optimum coupling with the RFQ, as at the crossover

the space-charge forces are more important, as confirmed by the measurements with a four-grid analyser. An optimal value of solenoid current for the operation with the EMU around 280 A has been found to avoid an excessive power density over the EMU sampler. Finally Fig. 26 shows the evolution of the emittance with the beam current increase; this confirms the influence of beam line pressure on the space-charge compensation (and thus on the emittance) by means of the injection of a controlled amount of argon into the beam line, as already done for the SILHI source for different gases.

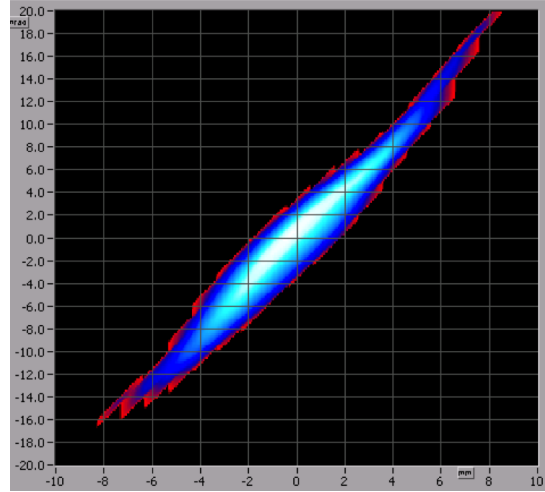


**Fig. 27:** Proton beam emittance measured without gas ( $P_{\text{source}} = 1.5 \times 10^{-5}$  mbar,  $P_{\text{line}} = 8.8 \times 10^{-6}$  mbar,  $I_{\text{extr}} = 32$  mA,  $\epsilon_{\text{norm}} = 0.069 \pi$  mm mrad).

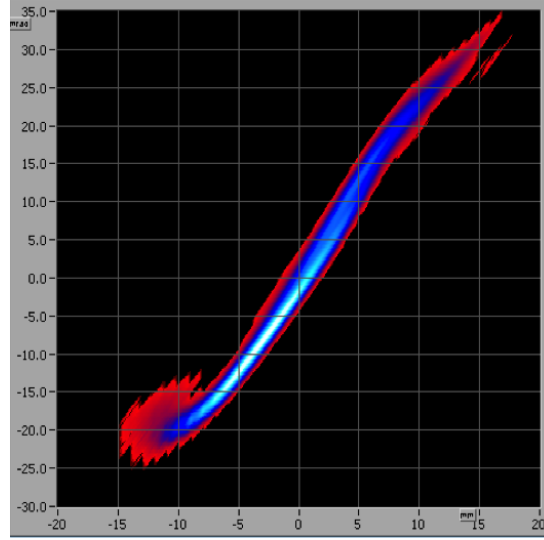
The measures have been carried out for fixed solenoid current (280 A) and puller voltage (40 kV) and by changing the discharge power from 450 to 650 W and the hydrogen flux from 0.45 to 0.59 sccm. It has been observed that the space-charge forces play a role for currents greater than 40 mA; the background pressure in that condition was around  $1.5 \times 10^{-5}$  mbar in the extraction column and around  $8.5 \times 10^{-6}$  mbar in the beam line. By adding an argon leak, the pressure increased to  $2.1 \times 10^{-5}$  mbar in the whole line, and a 30% beam emittance decrease was obtained without significant beam losses.

Figure 27 shows the emittance measured for the nominal current, while Figs. 28 and 29 show the emittance patterns for higher currents with and without gas injection.

In these cases the emittance growth is justified because of the lower space-charge compensation; then the benefits of argon injection are visible. In fact such gas injection improves the compensation and leads to lower value of emittance.

#### 4 Future perspectives

In the off-resonance microwave ion sources, the ECR is not a predominant condition for plasma generation; in fact, in this case higher electron densities can be obtained by means of a microwave discharge at higher magnetic field value and higher pressures. The plasma-cavity system is a distributed parameter resonant circuit, since the length of the plasma is of the same order of magnitude as the free-space electromagnetic wavelength. Then, differently from the ECR ion sources, the cavity diameter and excitation frequency are chosen to allow only one cavity mode to be excited for a given cavity length. In this case the power coupling into a given mode is usually accomplished by means of tuning stubs in order to achieve the necessary impedance match. The steady-state microwave discharge is characterized by the equality between the power absorbed by the plasma and the lost power, mainly due to inelastic ionization, excitation collisions and energy transmission out of the active discharge region. The power absorbed by the plasma is given by one-half of the real part of the complex Poynting vector, and therefore it depends



**Fig. 28:** Proton beam emittance measured without Ar ( $P_{\text{source}} = 1.9 \times 10^{-5}$  mbar,  $P_{\text{line}} = 1.1 \times 10^{-6}$  mbar,  $I_{\text{extr}} = 51$  mA,  $\epsilon_{\text{norm}} = 0.283 \pi$  mm mrad).

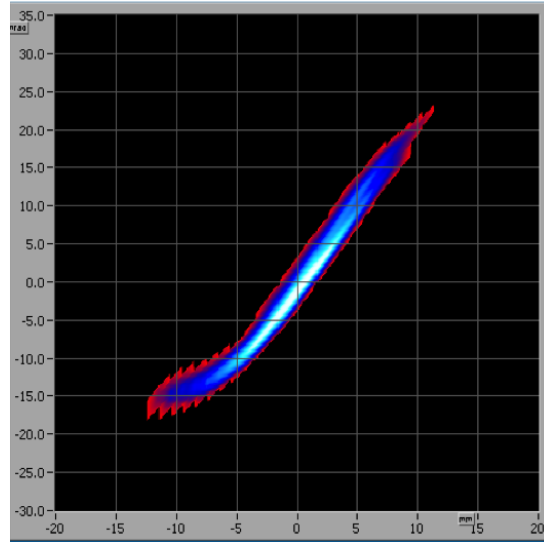


**Fig. 29:** Proton beam emittance measured with Ar ( $P_{\text{source}} = 2.45 \times 10^{-5}$  mbar,  $P_{\text{line}} = 2.2 \times 10^{-5}$  mbar,  $I_{\text{extr}} = 47$  mA,  $\epsilon_{\text{norm}} = 0.178 \pi$  mm mrad).

on the electric field strength in the plasma. In order to optimize the coupling for a given mode, the maximization of that electric field is therefore important. A waveguide transformer (usually maximally flat design) is widely used for such purposes for most microwave sources in operation nowadays. Such a device realizes a progressive matching between the waveguide, normally operating in the dominant mode, and the equivalent impedance of the plasma-filled chamber, also concentrating the electric field at its centre. Figure 30 shows a comparison of the electric field on the plasma chamber axis in the case that no transformer is used or by employing the TRASCO Intense Proton Source (TRIPS) or Versatile Ion Source (VIS) [16]. The excitation frequency is 2.45 GHz in all cases and it can be observed that an increase by a factor of 2 can be obtained, in the frequency range of circa 400 MHz, by appropriately shaping the waveguide ridges as discussed in detail elsewhere [17].

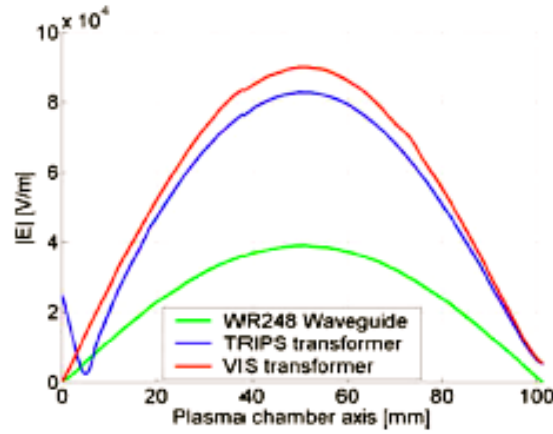


**Fig. 30:** Comparison of the electric field on the plasma chamber axis in different cases

Therefore, both matching transformers concentrate the electric field around its axis in a smaller region than the original WR 284 cross-section. This feature has been observed in the traces on the boron nitride disc at the injection side of the TRIPS and VIS plasma chambers, and it is particularly remarkable for the production of ion beams because the extraction system is centred on the axis of the plasma chamber and any enhancement of the plasma density at the centre of the cavity leads to a similar increase in the ion beam current. Even higher enhancements are made possible with such a device with different designs or by extending the ridge also within the span of the plasma chamber. Nowadays most of the high-intensity ion sources use automatic tuning units to optimize the power coupling into the operational mode and waveguide transformers similar to those previously described to enhance the plasma density inside the source. The increase in the latter parameter is mandatory for further increase in the produced currents.

Usually in microwave discharge ion sources used for intense beam production, the microwaves are provided by means of a waveguide located longitudinally with respect to the chamber axis. In these devices, the axis of symmetry of the magnetic field coincides with the chamber axis; this means that the injected wave is mainly an O or R wave when it propagates inside the plasma. However, because of the complex structure of the magnetic field lines, and because of possible reflections at the chamber walls, these modes may convert each other, and also X modes can be generated somewhere inside the cavity, through an O–X conversion. At that time, the X waves can be directly converted into a Bernstein electrostatic wave (BW) at the upper hybrid resonance (UHR) layer. BWs are a great advantage, as they travel into the plasma without any cutoff and provide heating even in the case of overdense plasmas. However, if the injection angle of the O mode is not optimal, the BW creation process has a low efficiency. The variations of the power and the background pressure change the plasma properties, and in turn affect the conversion efficiency. As BWs are known to be absorbed at cyclotron harmonics, the electrostatic wave generation in an MDIS is possible and can be used as an alternative plasma heating method. In order to increase the BW creation efficiency, the proper injection angle is needed: this can be achieved by using single cut antennas (waveguides) launching O waves in the right direction with respect to the magnetic field lines. In this way O–X–B conversion is possible, as observed in Ref. [18]. More details are discussed in Ref. [19]. A detailed investigation of this new approach to plasma heating in an MDIS may make it possible to take a large step towards higher extracted beam currents: in fact the key parameter in MDISs is the electron density, more so than the temperature (low charged ions are usually required), and by means of electrostatic wave heating we should be able to overcome the cutoff density at 2.45 GHz of a factor of 5 or 6.

## References

- [1] B. Wolf, *Handbook of Ion Sources* (CRC Press, Boca Raton, 1995).
- [2] N. Sakudo, *Rev. Sci. Instrum.* **49** (1978) 940.
- [3] J. Ishikawa, Y. Takeiri and T. Takagi, *Rev. Sci. Instrum.* **55** (1984) 449.
- [4] I.G. Brown, *The Physics and Technology of Ion Sources* (Wiley-VCH, Weinheim, 2004).
- [5] T. Taylor, *Rev. Sci. Instrum.* **63** (4), April (1992), 2507
- [6] J. Ishikawa, Y. Takeiri and T. Takagi, *Rev. Sci. Instrum.* **55** (1994) 449.
- [7] J. Sherman, A. Arvin, L. Hansborough, D. Hodgkins, E. Meyer, J.D. Schneider, H.V. Smith Jr., M. Stettler, R.R. Stevens Jr., M. Thuot, T. Zaugg and R. Ferdinand, Status report on a dc 130 mA, 75 keV proton injector (invited). *Rev. Sci. Instrum.* **69** (2) (1998) 1003.
- [8] P.-Y. Beauvais *et al.*, *Rev. Sci. Instrum.* **71**(3) (2000) 1413–1416.
- [9] J.-M. Lagniel *et al.* *Rev. Sci. Instrum.* **71**(2) (2000) 830–835.
- [10] R. Gobin *et al.* *Rev. Sci. Instrum.* **73**, (2002), 922
- [11] L. Celona, G. Ciavola, S. Gammino, R. Gobin and R. Ferdinand, TRIPS: the high intensity proton source for the TRASCO project. *Rev. Sci. Instrum.* **71** (2000) 771–773.
- [12] G. Ciavola, L. Celona, S. Gammino, M. Presti, L. Ando, S. Passarello, X.Zh. Zhang, F. Consoli, F. Chines, C. Percolla, V. Calzona and M. Winkler, A version of the Trasco Intense Proton Source optimized for accelerator driven system purposes. *Rev. Sci. Instrum.* **75** (2004) 1453–1456,.
- [13] F. Maimone, G. Ciavola, L. Celona, S. Gammino, D. Mascali, N. Gambino, R. Miracoli, F. Chines, S. Passarello, G. Gallo and E. Zappala, Status of the Versatile Ion Source VIS, Proc. 11th European Particle Accelerator Conf. (EPAC08), Genoa, Italy, 2008, MOPC151, 430.
- [14] R. Gobin, P.-Y. Beauvais, R. Ferdinand, P.-A. Leroy, L. Celona, G. Ciavola and S. Gammino, Improvement of beam emittance of the CEA high intensity proton source SILHI. *Rev. Sci. Instrum.* **70** (6) (1999) 2652.
- [15] L. Celona, G. Ciavola, S. Gammino, R. Gobin and R. Ferdinand, Status of the TRASCO proton source and emittance measurements. *Rev. Sci. Instrum.* **75** (2003) 5.
- [16] L. Celona, G. Ciavola, S. Gammino, F. Chines, M. Presti, L. Ando, X.H. Guo, R. Gobin and R. Ferdinand, *Rev. Sci. Instrum.* **75** (2004) 1423.
- [17] L. Celona *et al.*, *Rev. Sci. Instrum.* **81** (2010) 02A333.
- [18] H.P. Laqua, W7-AS Team and ECRH Group, *Plasma Phys. Controlled Fusion* **41** (1999) A273.
- [19] H. Laqua, M. Otte, Y. Podoba, D. Mascali, S. Gammino, L. Celona, G. Ciavola, N. Gambino, R. Miracoli and F. Maimone, Study of the Bernstein wave heating in the WEGA stellarator plasma and possible application to ECRIS, INFN, Report No. INFN/AE-09/1 (2009).